

# MACAO-VLTI Adaptive Optics Systems Performance

R. Arsenault, R. Donaldson, C. Dupuy, E. Fedrigo, N. Hubin, L. Ivanescu, M. Kasper, S. Oberti, J. Paufique, S. Rossi, A. Silber, B. Delabre, J.-L. Lizon, P. Gigan<sup>†</sup>

European Southern Observatory (ESO), Karl-Schwarzschild-Str. 2, 85748 Garching bei München, Germany

<sup>†</sup> LESIA, Observatoire de Paris-Meudon, 5 Place Jules Janssen, 92195 Meudon, France

## ABSTRACT

In April and August '03 two MACAO-VLTI curvature AO systems were installed on the VLT telescopes unit 2 and 3 in Paranal (Chile). These are 60 element systems using a 150mm bimorph deformable mirror and 60 APD's as WFS detectors. Valuable integration & commissioning experience has been gained during these 2 missions. Several tests have been performed in order to evaluate system performance on the sky. The systems have proven to be extremely robust, performing in a stable fashion in extreme seeing condition (seeing up to 3"). Strehl ratio of 0.65 and residual tilt smaller than 10 mas have been obtained on the sky in 0.8" seeing condition. Weak guide source performance is also excellent with a strehl of 0.26 on a V~16 magnitude star. Several functionalities have been successfully tested including: chopping, off-axis guiding, atmospheric refraction compensation etc. The AO system can be used in a totally automatic fashion with a small overhead: the AO loop can be closed on the target less than 60 sec after star acquisition by the telescope. It includes reading the seeing value given by the site monitor, evaluate the guide star magnitude (cycling through neutral density filters) setting the close-loop AO parameters (system gain and vibrating membrane mirror stroke) including calculation of the command-matrix. The last 2 systems will be installed in August '04 and in the course of 2005.

**Keywords:** Adaptive Optics, Curvature, Bimorph, Real-Time-Computer, Piston

## 1. INTRODUCTION



Figure 1: MACAO-VLTI on the Coude platform. The arched structure support M9, the dichroic reflecting light to the VLTI and transmitting the visible to Macao. The WFS can be seen under the arch. The shiny cryostat on the upper left is the ITC.

The ESO Adaptive Optics Department (part of Telescope Systems Division) decided in 1998 to undertake an active adaptive optics program aimed at feeding several ESO instruments with wavefront corrected beam<sup>1,3,7,13</sup>. In particular the VLT Coude focii needed to be equipped with low cost adaptive optics to help beam recombination of the VLTI<sup>2</sup>. Four identical copies of this instrument are being built; one for each VLT. The first two MACAO-VLTI systems have been delivered, installed and commissioned in April and August '04 respectively. This paper describes the on-sky performance of the individual systems (for interferometric performance see<sup>11</sup>). A complete presentation of the design can be found in<sup>4</sup>.

Both MACAO-VLTI on UT2 and UT3 required approximately 30 days to be unpacked from the crates, installed re-integrated and calibrated followed by one week of sky tests. The latter aimed at evaluating the performance of the AO

systems in real observing conditions but also at testing several instrumental functionalities.

## 2. TEST DESCRIPTIONS AND TEST TOOLS

### 2.1. Instrumental Functionalities Tests

Several instrumental functions must be tested to insure proper operation and use of the system in the telescope environment.

- XY Table calibration: The XY table is used to move the WFS box in the Coude focal plane for off-axis star acquisition and guiding. The calibration consists in defining the scale (mm per arcsec) and orientation of the XY table with respect to the cardinal points on the sky. This is done by acquiring stars first close to the optical axis and then the parameters are refined as one acquires stars further away, up to the 1 arcmin radius (~110 mm)
- TCS (Telescope Control System) offloads: When the deformable mirror gets close to saturation in tilt or focus, a command is sent to the TCS to tip the telescope or change its focus value. Orientation of the tilt and scale of tilt and focus must be calibrated.
- Star acquisition: Once the telescope has completed a pointing and applied an active optics correction, the star is acquired by MACAO-VLTI. The procedure tested is the following and one simply makes sure no glitch occurs during the process. Telescope pointing is accurate enough to get the star in the 2-3 arcsec field of view of the WFS. The most absorbing Neutral Density filter is selected. Shutter is opened and APD counts monitored. If signal a preset minimum, a less absorbing ND filter is selected and the process continues until a count rate minimum < cnt rate < maximum is reached. Shutter is closed. The system evaluates the Star magnitude (knowing the absorption of the filter and using a known calibration between count rate and V magnitude) and select the AO loop main gain (according to a lookup table). The seeing monitor value is read and a membrane stroke is selected (according to a lookup table defined during laboratory tests). Then the shutter is opened again and the AO loop is closed.
- Scales: the various scales mm/arcsec are measured for the ITC, TCCD in mode direct and large field.
- Atmospheric refraction compensation: A standard algorithm is used in Paranal to correct for the difference of position of astronomical targets versus the wavelength of observation. The hardware implementation is checked. A set of sources are pointed at various azimuth and zenithal angles; AO loop is closed. Position is measured on the ITC w/o refraction compensation and then with refraction compensation.
- Throughput: The actual throughput of the instrument is calculated using photometric standards.
- Off-axis guiding: A star is acquired on the ITC center field. Another star is acquired off the center field (offset calculated from coordinate difference). The loop is closed on the off-axis object and regular images are taken on the ITC. The RMS position deviations of the on-axis star are deduced from the images. This test is usually performed at meridian crossing and close to zenith where the azimuth rotation is fastest.

### 2.2. AO related Tests

#### 2.2.1. Performance Tests

The performance tests aim at obtaining the data necessary to plot a curve Corrected Strehl ratio versus guide star V magnitude. The AO system parameters i.e. main loop gain and membrane stroke are set to best values as calibrated in the laboratory. Then they are varied by  $\pm$  one step in order to find an optimum (procedure is more to insure laboratory values are correct). In order to average out the seeing variations a sequence of 72 randomly arranged configuration of main loop gain and membrane stroke are used each one taking 3 possible values. The result is a set of data: main loop gain (3 values), membrane stroke (3 values) and seeing (continuously varying) and corresponding K (2.2  $\mu$ m narrow band) images for each configuration.

We aim at covering seeing values from 0.5'' to 1'' and star magnitudes  $V > 10$  to  $V \sim 16$ . The initial specification can be found in<sup>4</sup> and is a K-band strehl > 50% for  $V < 8$ , >25% for  $V = 15.5$ ; this for seeing of 0.65'' (0.5  $\mu$ m) and wind speed of 10 m/s.

#### 2.2.2. AO loop residual jitter

The beam combination at the VLTI is done using monomode optical fibers spatial filtering. Basically, MACAO-VLTI must provide an optimal flux injection in the fibers. The main criteria is high strehl but also a stability of the corrected

image position. A residual jitter specification has been defined at 10 mas RMS. This is tested by taking a sequence of short exposures with the ITC (16Hz acquisition) and calculating the RMS deviations from the average centroid.

### 2.2.3. AO Stability and flexibility tests

Other tests are carried out in order to test the flexibility of the system. A quantitative evaluation of performance is not always possible for such tests.

- **Stability:** AO loop closed on star for substantial amount of time at largely varying zenithal angle. Loop closed in extremely bad seeing conditions. Loop closed with laboratory obtained interaction matrices. Results of the tests are of a binary nature whether the loop remain stable or not.
- **Extended Sources:** Extended sources are observed to see the capacity of the system to remain stable with non point source target. Galaxy nuclei, planets, proto-star nebulae etc. It is often difficult to measure size of structure but in some case planet edge or fine structure can be seen and provide some angular measurement on the corrected image.
- **Double star:** Whether correction is satisfying with 2 targets in the WFS field of view.

### 2.2.4. Piston Performance

Another important requirement is to maintain to a minimum the piston artificially introduced by the deformable mirrors of 2 independent MACAO-VLTI, running on different Unit Telescopes. Such effect would reduce the fringe contrast at the recombination laboratory and be detrimental to the performance of the Interferometer.

The piston mode removal algorithm implemented had been first described in<sup>6</sup>. Most of the piston characterization & tune-up takes place in the laboratory where a setup has been designed in order to do so. Then a final check is done on the telescope to confirm the level of correction in situ. For details about laboratory characterization and performance on the sky see<sup>10,11</sup>.

## 2.3. Calibrations

### 2.3.1. Calibration Setup

MACAO-VLTI being located at the Coude focus and a number of Coude train mirrors are located upstream from the WaveFront Sensor (WFS) box. The point source used for all calibrations (Interaction Matrices and more) is a 10  $\mu\text{m}$  optical fiber that can be inserted at the Nasmyth focus just in front of M4. The WFS sensor is located below a dichroic sending the infrared (IR) light (1 to 13  $\mu\text{m}$ ) to the VLTI and using a fraction of the visible light (~53% from 0.4 to 0.9  $\mu\text{m}$ ) for WF sensing. This dichroic is the 9<sup>th</sup> optics in the Coude train.

It is worth mentioning that the MACAO-VLTI WFS is NOT mechanically mounted on the telescope the way a Nasmyth or Cassegrain adaptive optics instrument is. It is mounted on the Coude platform while the telescope, and deformable mirror, are rotating above on the azimuth axis. The only problem observed due to this particular configuration was that an important level of internal turbulence was observed right after the installation and integration activities. It was mainly due to an important chimney effect between the Coude room (then heated by human activities and halogen spotlights) and the azimuth platform. It usually stabilized after one night observation and later observation of the calibration source at night time showed a rock steady beacon with extremely low level of internal turbulence. Excellent interaction matrices could then be obtained.

### 2.3.2. Calibrations Performed

The list below describes the calibrations required for the functioning of the system and a brief description. All uses the Nasmyth calibration source. Note that the membrane mirror is an aluminized silicon membrane set in vibration (alternating concave and convex shape) by a loudspeaker at 2.1 kHz. Its purpose is to produce the in and out focus image of the pupil on the lenslet array.

- **Membrane mirror stroke calibration:** The membrane mirror being driven by a sine wave, this calibration aims at finding the relation between driving voltage and minimum radius of curvature (or highest optical gain). The calibration source is tilted by the maximum field of view of the wavefront sensor for a 0.5 m curvature radius of the membrane. This value, obtained from the optical model of the WFS optics, is 0.4'' radius. The calibration source is

placed at this value off the center. Tilt signal is monitored as the membrane stroke increases (radius of curvature decreases). The tilt signal saturates when the radius of curvature reaches 0.5 m.

- Membrane mirror phaselag adjustment: This is the optimal phase difference between the counting of the APD pulses and the sine wave driving the membrane mirror. A tilt signal is generated on the calibration source. This is usually done by tilting the DM. The amplitude of the tilt signal is measured and the system changes the phaselag in order to cancel the tilt signal. When the zero value is found,  $\pi$  is subtracted to the phase found and used for optimal phaselag.
- Interaction Matrices: The methodology to obtain interaction matrices has evolved since the first MACAO system has been tested. The method actually used has proven to give the best results in terms of minimizing the saturation of the tilt electrodes on the Deformable mirror (substantial improvement). It consists in an iterative process where one defines a set of system modes to activate and measure instead of a simple zonal activate and measure process. Speed of measurement, integration time has little effect as long as the photon signal to noise ratio is sufficiently high. Several interaction matrices are obtained for a given number membrane mirror stroke (at least 5). For a continuous sampling of the membrane mirror stroke an interpolation of the matrices is used. See<sup>9</sup> for a more exhaustive description.
- DM flattening: This aims at finding the voltage vector that corrects for the static aberration of the DM (when 0 volt is applied to all electrodes). The procedure simply consists in closing the AO loop w/o turbulence and using a very low main loop gain (~1%) and recording the voltages. The name of this procedure can be misleading since as a result the DM is not necessarily flat but will adopt the shape needed in order to minimize the optical aberration of the whole optical system (Nasmyth calibration source down to the M9 dichroic- telecentric lens)

## 2.4. Infrared Test Camera



A test camera was especially built to characterize all MACAO systems. The camera used an optical module made of 3 spherical diamond turned metallic mirrors. It was an internal development including detector controller (IRACE), acquisition software & cryogenics. For the first 2 commissionings an engineering grade Hawaii chip was used with 2 operational quadrants. This configuration provided a field of view 13.6x6.8 arcsec and a pixel scale of 0.0133"/pix. The field of view rotation (at Coude) was not compensated for but exposures were short in comparison with the rotation rate.

The Strehl ratio obtained on a calibration source located at the Nasmyth focus was 0.91 due to the camera optics. The strehl ratios measured on our astronomical targets were thus divided by this value to provide a strehl ratio as provided by the adaptive correction.

Figure 2: The ITC. One sees the opening in the Coude room ceiling allowing passage to the Coude optical beam. The black box just below contains the M9 dichroic. Two 45 flat mirrors intercept the Coude beam to feed the ITC. The shiny bare aluminum parts are the body of the ITC; the square box contains the optics and detector while the cylindrical tank on the right is the liquid nitrogen bath.

## 3. TEST RESULTS

### 3.1. Functional Tests

All functional tests were successfully carried out and results were satisfactory. Of particular interest were the ones of precision of the calibrations related to AO performance.

The RoC (Radius of Curvature) to voltage calibration accuracy for the membrane mirror gave a typical RMS error of the Voltage to RoC calibration of 5%. It appears to be entirely negligible; this is 1/10 of the step used to interpolate between the various command matrices (obtained for different RoC).

The Phaselag calibration showed RMS variations of the Phase lag: 1.5°. Such variations measured in the phase lag are consistent with a 2°C temperature variation and correspond to a  $\pi/120$  phase variation ( $\pi/40$  has been estimated as negligible).

Another test consisted in measuring the stability of the DM flattening procedure. A stability 22 nm RMS up to 60 min was measured. The specification is for open loop evolution (<120nm for 5 min.). Actual measurement was difference between calibrations, which is slightly different.

### 3.2. Chopping Tests

The chopping tests constitute an important functionality for MACAO-VLTI but are very demanding on the adaptive optics system. Extensive tests have been conducted and a substantial investment has been made since the design of MACAO-VLTI to accommodate this functionality.

The basic difficulty consists in synchronizing MACAO-VLTI RTC with the chopping cycles of the secondary mirror of the 8m telescope. The AO loop must be closed while the target is on-axis and opened when the telescope looks off-axis. The specification was issued for a chopping cycle of 1 Hz with a goal of 5 Hz. Both were met, and the plots below show the 5 Hz measurements.

The following figure shows the data taken UT3 on the 8<sup>th</sup> August 2003 (Seeing 0.6-0.7"). The plots show very good stability and synchronization.

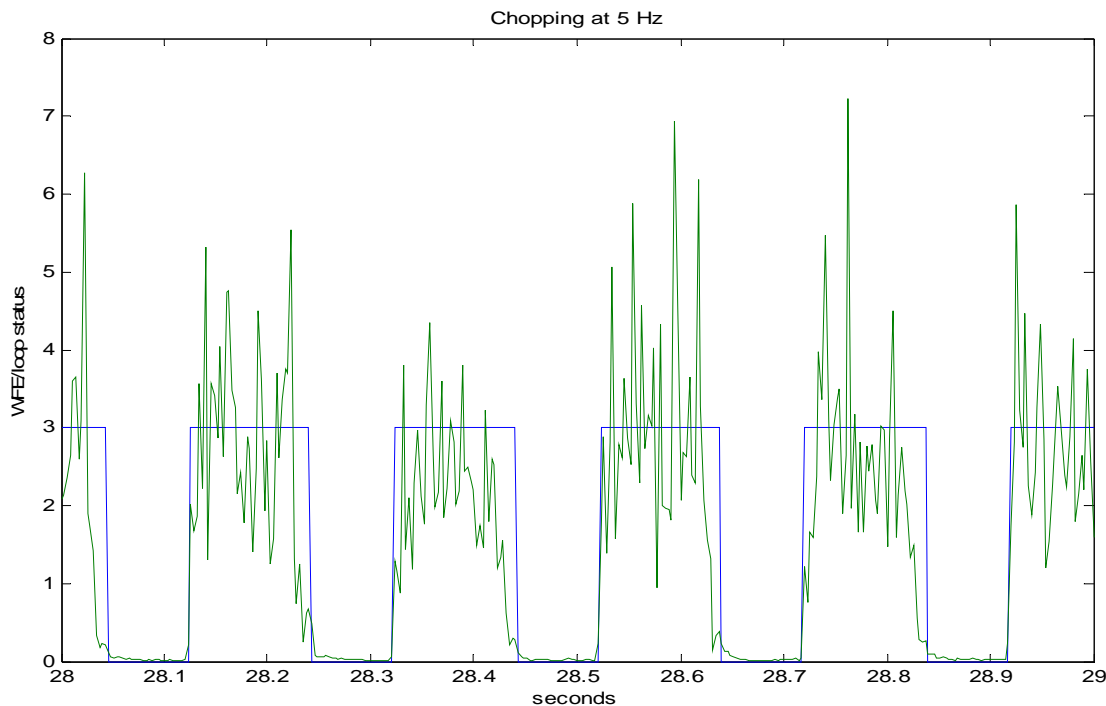


Figure 3: Chopping at 5Hz. Wavefront error and loop status

One sees a large WF residual error on the off-axis part of the cycle; this is because the AO loop is opened then and residual WF error reflects the opened atmosphere seeing. During the off-axis cycle the MACAO-VLTI deformable mirror keeps the shape it had when the loop was opened. As soon as M2 brings back the target, the wave-front error decreases. The convergence of the loop at the start of the on-axis part of the cycle is very fast in the 5Hz case (compared to 1 Hz) because the deformable mirror is in a position that was correct just one tenth of second before. A few control loop cycles reduce substantially the WF error.

Figure 4 shows the evolution of wave-front error close to a loop state transition. The big dots right before and after the transition marks 20 milliseconds to take into account the motion of M2. When M2 is chopping the wave-front sensor is looking at sky and thus does not have any valid signal.

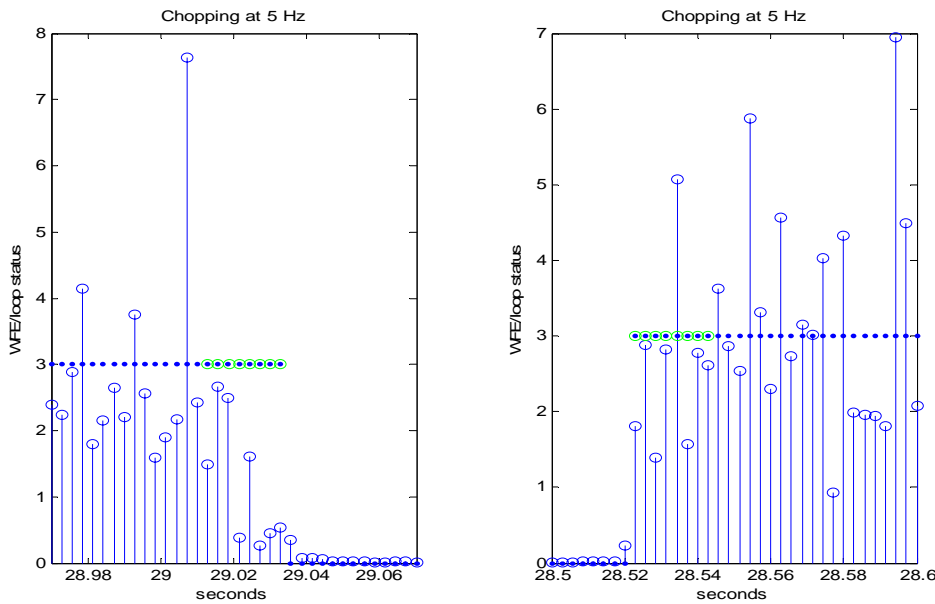


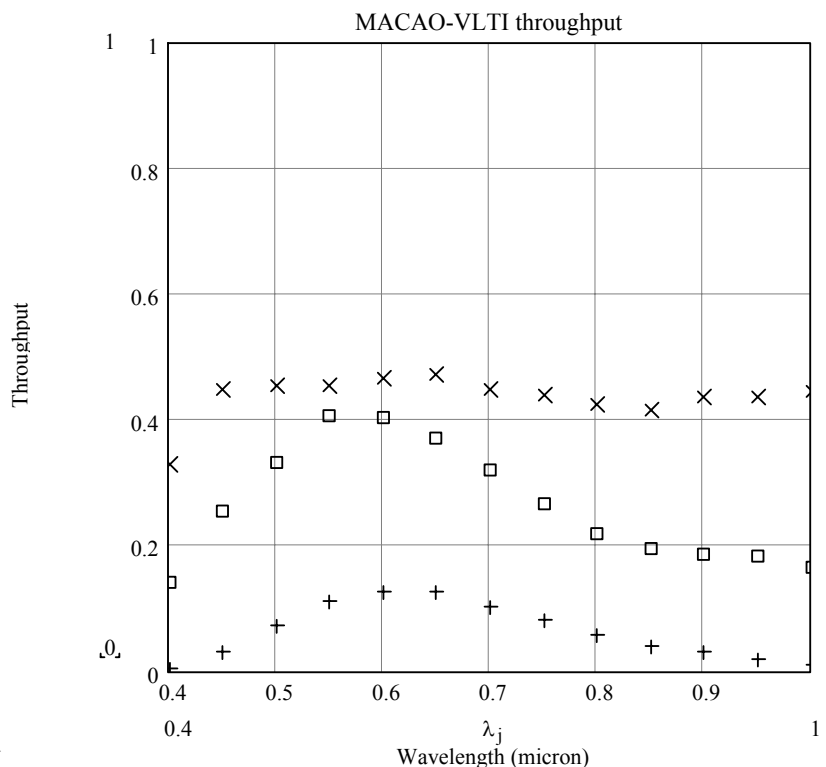
Figure 4: Chopping at 5 Hz. Detail of start and end of a cycle

manufacturers of optical components.

An ad hoc aging factor has been used for the telescope and Coude optics. Also some optical interfaces suffer from an unknown loss that has been estimated: coupling of the second lenslet array to the entrance of the optical fibers and coupling of the fibers end to the APD photo-sensitive array. With such assumption the following throughput curves have been obtained (see Figure 5).

A variety of stars of different magnitude and colors were observed during the commissioning on different nights and always in photometric conditions. The total number of photons measured by the WFS was ~20% lower than what expected from the curves shown in Figure 5. The reason for this is likely that some

Figure 5: Throughput curves of the telescope optics including Coude train and dichroic ("x"), of the WFS itself (box), and total (plus signs).



In conclusion the chopping mode of MACAO-RTC has been fully tested and verified. Requirements are fully met and also the goals. Stability is very good. Time to re-close the loop is very short, at least on the bright star used for the test and the good seeing conditions

### 3.3. System Characterization

#### 3.3.1. System Throughput

The total throughput has been calculated by multiplying all transmission and reflection curves provided by the

photons are vignettted by the action of the vibrating membrane mirror, especially at high stroke. Between open loop and close loop 15-20% of the flux is lost due to this effect (measured in the laboratory).

### 3.3.2. Transfer Function

We want to estimate the error-rejection function, so the ratio between the (statistical) Fourier transform of the output wavefront with the input wavefront. We compute the same ratio using the curvature signal measured by the sensor. Ideally one should record the input curvature and the output curvature sequence at the same time. Unfortunately this is not possible and one can only measure an open loop and a close loop time series and assume the conditions are the same.

We took the two sequences one right after the other and stored them in the same file. A status flag show which part of the file contains open loop data and which closed loop data.

Another difficulty is added by the high non-linearity effects that the closed-loop action adds. In closed loop the system goes very frequently in over-voltage condition on the deformable mirror. The system reacts to this condition by saturating the voltage on the corresponding electrodes thus introducing a non-linear effect, which is naturally observed and recorded on the sensor, so on our curvature sequence. The transfer function being a linear relationship, our estimation will be biased.

The electrode saturation effect is much stronger on the external electrodes. The WFS geometry is such that 40 electrodes/sub-apertures are located within the pupil area and 20 are outside. The latter are called the tilt electrodes since they do not produce curvature inside the pupil but only a tilt. The MACAO-VLTI mirror has tilt electrodes area smaller than what has been used conventionally for bimorph mirrors. They extend to a radius of 1.5 times the pupil radius while in the past one has used 2 times the radius of the pupil (Initial Roddier's 13-element system, PUEO 19-element at CFHT, SINFONI).

Another detrimental effect to using the external ring of sub-aperture for this calculation is that the lenslet of the external ring have the largest sag. This is very difficult to produce and the design incorporate some fresnel transitions to make the maximum sag lower.

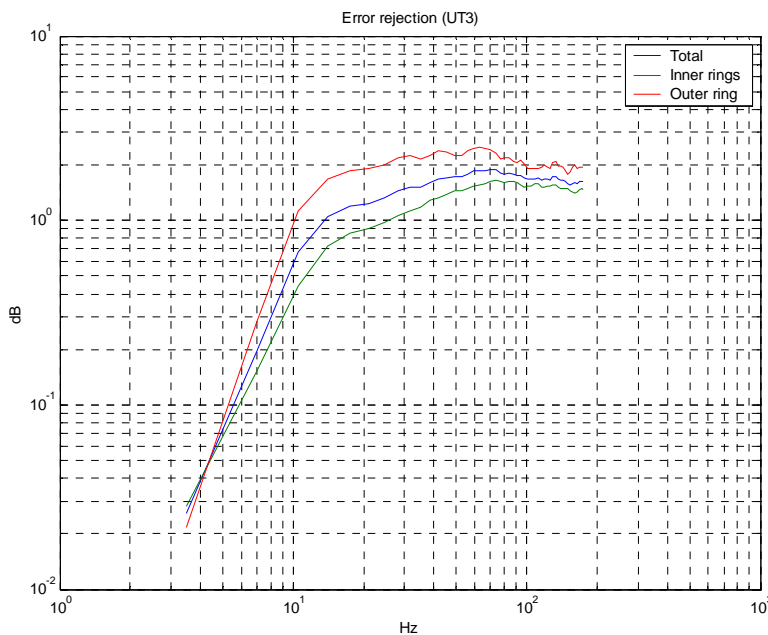


Figure 6: Transfer function of MACAO-VLTI. The higher curve represent the ring of apertures/electrodes outside the pupil (external) the lower curve the ones inside the pupil (inner) and the middle curve average of both. If one considers the inner electrodes (non-saturated) the bandwidth of the system is 28 Hz.

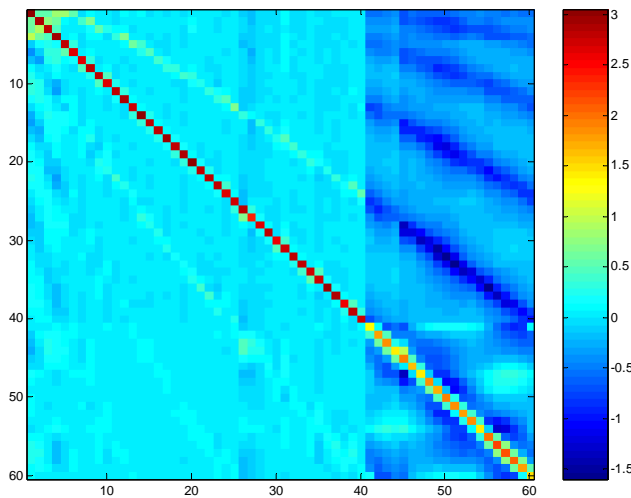
Furthermore, the fabrication process produces more irregular surface and therefore, diffusion for large sag lenses. The end result is that the throughput of the external ring of electrodes is lower, leading to noisier curvature signal. These 2 effects contribute to a higher rate of saturation of the external tilt electrodes and biases the bandwidth measurement to lower values. We believe the inner electrodes provide a closer to reality bandwidth measurement; the value thus obtained is very close to the simulated value of ~35 Hz (0 dB).

### 3.3.3. Interaction Matrix Calibration

The interaction matrix (IM) calibration is an important step in order to insure an optimal performance of the AO system. Care has been taken to find the best combination of parameters to obtain it. Several IM must be obtained for typically 5 different RoC of the membrane mirror. In order to allow the use of any RoC, an interpolation of the 5 IM's is done. The parameters that must be adjusted are:

- the stroke applied on the deformable mirror: up to 10 % of full amplitude ( $\pm 400$  V)
- the integration time per channel
- the time to skip between voltage applied and curvature measured
- the total number of cycles (how many global IM measurements to average)
- the method; zonal, Hadamard, iterative system modes

A number of undesirable effects have driven the choice of the above parameters like: non-linearity of curvature WFS, DM stabilisation time after a step voltage application, hysteresis, creep, photon noise, non-linearity of the DM stroke.



The Figure 7 shows one of the best IM. The SNR is a criteria of homogeneity of the inter-diagonals zone in the IM while the CCN is the so-called conditioning number, the ratio between the smallest and largest eigen values of the inverted matrix (command matrix).

Other methods have been explored like using a Hadamard matrix instead of a zonal one (pushing one actuator at a time). The Hadamard matrix has interesting properties like maximizing the curvature signal for a given DM electrode voltage. However, MACAO is mainly suffering from the WFS non-linearity, an a method using system modes has the advantage of providing a more uniform curvature signal for each mode (voltage vector can vary a lot from mode to mode). This iterative method gave the best results and was developed during the SINFONI integration & test phase in Garching.

Figure 7: One of the best IM obtained with parameters: 80 cycles of 0.045 sec integration time per channel and 0.025 sec skip time. The DM stroke was 15%, conditioning number 30 and SNR of the IM 78.

For more details and improvements see<sup>9</sup>.

### 3.4. Strehl Ratio, Residual jitter & Image Correction

The strategy of this test has been previously described in section 2.2.1. The Figure 8 summarizes all the results:

- Diamonds show the specifications;
- The dot line is the result of computer simulations;
- The solid line represents measured values in the laboratory with artificially produced turbulence;
- The boxes are values measured on the sky in April '03 on VLT unit 2;
- The circles are values measured on the sky in August '03 on VLT unit 3 (error bars indicates lower limits on the values when the seeing was substantially worse than the specified value of 0.65")
- The dash-dot line shows the open loop strehl in the laboratory setup

In all cases the specifications are met. A first surprising results is that the simulated curve is worse than many measurement on the sky and in the laboratory. This has been explained by the vibrating membrane mirror stroke which

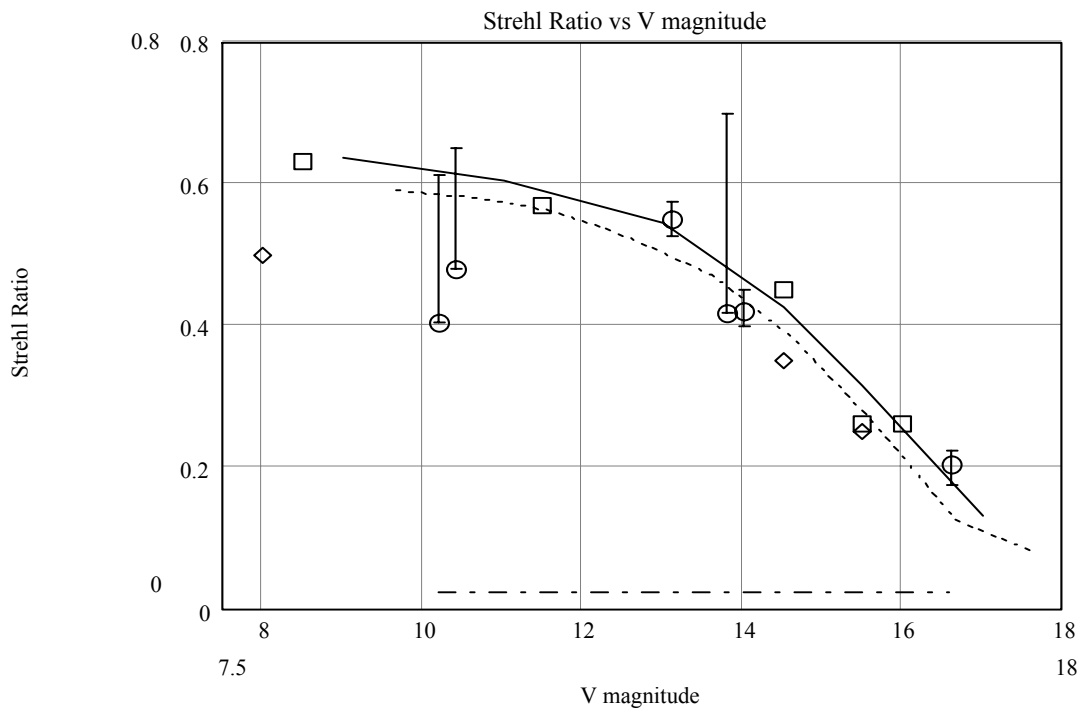


Figure 8: Strehl ratio versus guide star magnitude; simulated and observed data.

was not optimal during simulations. By using the same membrane stroke as in the simulation one finds the same strehl ratio as on the dot curve.

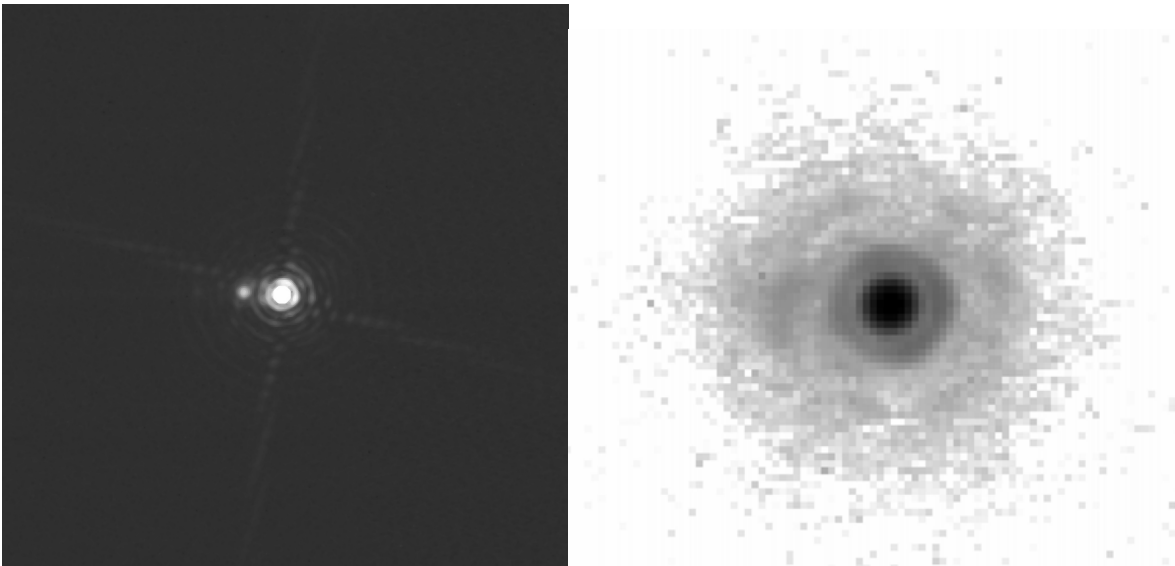


Figure 9: Image of the calibration beacon at the telescope as seen by the ITC at the Coude focus (left). The strehl measured in 91% (no turbulence). The image on the right is the highest strehl observed, 65%, during both commissionings (April and August '03; see text for details).

On Figure 9 (right hand side) one sees the best diffraction limited image obtained during the August '03 commissioning on UT3. The star HIC83577 (mag 9.87) was observed with a seeing of 0.8 arcsec. The loop has been closed with a

boosted diagonal interaction matrix, 28.5 cm of radius of curvature on the membrane mirror and a loop gain of 90% (10% offload gain to the Tip-Tilt mount). The final image is the average over 64 pictures integrated 1sec each. Despite this seeing of 0.8 arcsec, the strehl ratio is 58%. If we take into account the quality of the ITC, i.e. 91% on the beacon, this means that the correction performance amounts to 65% under these conditions. The full width at half maximum is 4.7 pixels i.e. 63 marcsec.

The residual jitters obtained on sequences on narrow K-band images. The star HD1685 (mag 5.5) has been observed in closed loop and with the ITC using very short exposure times. Thus, it is possible to compute the residual jitter for a high temporal frequency. For 128 exposures of 0.062 seconds, the residual jitter is 4.5 marcsec rms i.e. less than the specification of 10 marcsec. Therefore, the system fulfils the specification at a high temporal acquisition frequency.

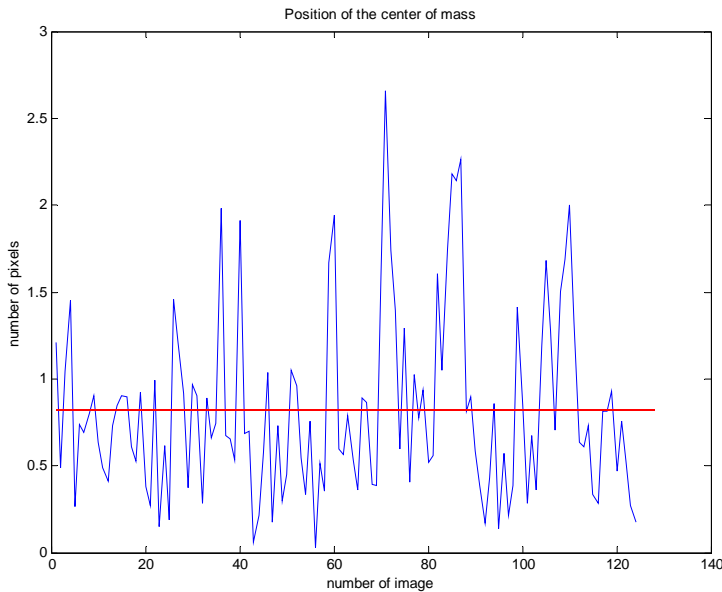


Figure 10: Jitter of the centroid of the diffraction limited image on a sequence of 128, 0.062 msec images. The vertical axis units are pixel (0.0133 "/pix).

Among the spectacular targets observed during the commissioning runs were the Galactic Center and Neptune.

Below (Figure 11) a corrected image of the galactic center in K band. This image compares advantageously with other taken by larger telescopes and AO systems with larger number of actuators. This is a 90-second exposure of the central 6 x 13 arcsec<sup>2</sup> around the Galactic Center obtained under average atmospheric conditions (0.8 arcsec seeing). Although the 14.6 magnitude guide star is located roughly 20 arcsec from the field center - this leading to isoplanatic degradation - the present image is nearly diffraction limited and has a point-source FWHM of about 0.115 arcsec.

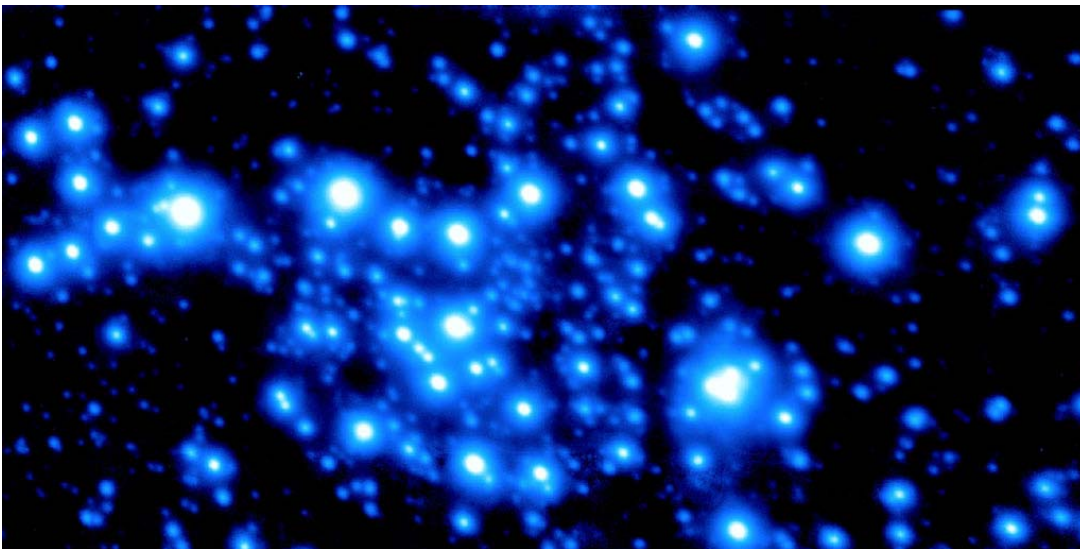


Figure 11: The Galactic Center observed in K-band (see text for details).

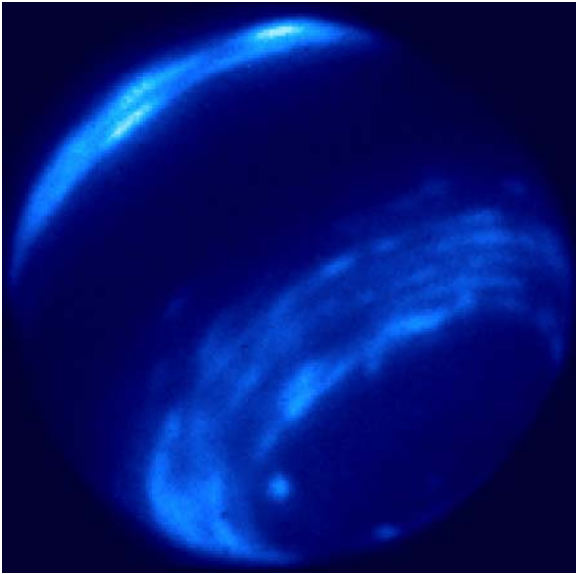


Figure 12: H-band image of Neptune (see text for details). Planet diameter is 3" in size.

The Neptune image has been obtained by combining 30 images acquired with 10 seconds of integration time (i.e. 5 min total). The acquisition of the set lasted 7 min 40 sec, knowing that in 6 min. the angular rotation of Neptune at its equator corresponds roughly to 0.4" of blur. Neptune itself was the guide source (3" diameter) and the finest details are 0.067" in size (FWHM).

### 3.5. Piston Performance

Considerable progress has been made on the piston issue since the last measurements done on the telescope in August 2003. The 3<sup>rd</sup> MACAO-VLTI system actually being tested in the laboratory (until May '04) has been used to get more insight in the piston behavior and how to improve the previous performance.

Several factors have a major influence on the piston performance; the real time control frequency, the type of control matrix, the overvoltage rate (or DM saturation) and of course the seeing during the close loop correction. The control frequency has been changed from 350 to 420 Hz which has been shown to reduce tremendously power injected at the main

resonance of 680 Hz. Since a large contribution to piston comes from this resonance, a substantial gain has been accomplished through this change. Besides, going to a higher control frequency has advantages like increasing the bandwidth and allowing more latitude on the adjustment of the system main gain (smaller gain values still produces a good corrected Strehl ratio).

It has been observed that the piston over the pupil is not a linear function of the electrode voltage. A second order fit to the curve piston versus voltage provides a much better description of the data. Assuming a linear behavior leads to an error of 3% at 100 V and 13% at 400 V (maximum voltage); note that these values differ slightly from an electrode ring to another (different surface area).

Substantial improvements have been accomplished through the use of a better interaction matrix. Initially a large number of saturations of tilt electrodes have been observed on the sky. This was due in part to a "checker-board" type of mode being applied on the tilt electrodes (alternately large positive and negative stroke on adjacent electrodes along the circumference). Since the tilt electrodes are used to correct the piston, this had a large detrimental effect. In the meantime, alternate and better ways of obtaining the interaction matrix have been implemented which have completely eliminated this checker-board type and greatly reduced the voltage saturation on DM. For details on these interaction matrix measurements see<sup>9,12</sup>. The table below summarizes the performance after various type of improvements:

Piston (nm RMS)	Date	System Configuration Laboratory results
164	June '03	MACAO#3, Zonal IM; LCF 350 Hz; non-linear PRA
80	Feb. '04	Modal IM; LCF 350 Hz; non-linear PRA (IM were still not optimal)
25-75	April '04	Modal IM; LCF 420 Hz ; non-linear PRA (Smaller contribution from resonance peaks)
20-65	April '04	Modal IM; LCF 420 Hz; non-linear PRA; non-linear piston measurement (Less voltage saturation on the external ring of electrodes. Adjustment of the main loop gain allow to decrease piston while preserving strehl above specified value of 50%)
<b>IM:</b> Interaction Matrix, <b>PRA:</b> Piston Removal Algorithm, <b>LCF :</b> Loop Control Frequency,		

For more details on the piston characterization and correction see<sup>10,11,12</sup>.

#### 4. CONCLUSIONS

The MACAO-VLTI systems are still in the fabrication/commissioning stages. Two have been installed and commissioned on the VLT Unit Telescopes #2 and #3 in Paranal. The third system will be commissioned on UT4 in August 2004, while the fourth and last system will be delivered in mid-2005.

The results of the laboratory and on-sky tests show that the MACAO-VLTI systems fulfill all specifications. Furthermore, use in real environment conditions revealed a robust and user friendly system that can be operated by non-AO specialists (Telescope Operators).

The key results are strehl ratio of  $\sim 0.65$  in K-band in seeing condition up to  $0.8''$  for bright sources ( $V < 10$ ). The limiting magnitude is  $V \sim 16$  where a strehl ratio of 0.26 in K has been obtained. Observations of extended source have been obtained on galaxy nuclei, nebulae and planets. Observation of Neptune (planetary disk of  $3.0''$ ) showed striking atmospheric bands  $0.067''$  in size.

After a total of 20 nights on the sky, observation in bad seeing conditions (up to  $3''$  FWHM), with various quality of interaction matrices, no more than one or two times did the system loop opened for unexplained reason. Same interaction matrices were used at 4 months interval showing a similar performance and minimizing the need to recalibrated the system. We interpret these as signs of reliability and robustness.

#### ACKNOWLEDGMENTS

The MACAO team wishes to thank the ESO Paranal director's office which has been very supportive of our commissioning efforts and the ESO Paranal staff for their enthusiastic and competent support.

#### REFERENCES

1. H. Bonnet, S. Ströbele, F. Biancat-Marchet, J. Brynnell, R. Conzelmann, B. Delabre, R. Donaldson, J. Farinato, E. Fedrigo, N. Hubin, M. Kasper, M. Kissler-Patig, 2003, SPIE **4839**: Adaptive Optical System Technologies II, p. 329
2. A. Glindemann, J. Algomado, R. Amestica, P. Balester, B. Bauvir, E. Bugueno, et al., 2003, Proc. SPIE **4838**: Interferometry for Optical Astronomy II, p. 89
3. A.F.M. Moorwood, P. Biereichel, J. Brynnell, B. Delabre, R. Dorn, G. Finger, F. Franza, G. Huster, Y. Jung, H.-U. Kaeufl, et al. 2003, Proc. SPIE *Astronomical Telescopes and Instrumentation*, p. 944
4. R. Arsenault, J. Alonso, H. Bonnet, J. Brynnell, B. Delabre, R. Donaldson, C. Dupuy, E. Fedrigo, J. Farinato, N. Hubin, L. Ivanescu, M. Kasper, J. Paufique, S. Rossi, S. Tordo, S. Ströbele, J.-L. Lizon, P. Gigan, F. Delplancke, A. Silber, M. Quattri, R. Reiss; 2003, Proc. SPIE **4839** Adaptive Optical System Technologies II, P.L. Wizinowich, D. Bonaccini, Ed. P. 174-185
5. F. Roddier, 1988, "Curvature sensing and compensation: a new concept in adaptive optics" Appl. Opt. **23**, 1223-5
6. C. Verinaud, F. Cassaing, 2001, Astron. & Astrophys. **365**, 314
7. N. Hubin, R. Arsenault, H. Bonnet, R. Conan, B. Delabre, R. Donaldson, C. Dupuy, E. Fedrigo, L. Ivanescu, M. Kasper, M. Kissler-Patig, J.-L. Lizon, M. Le Louarn, E. Marchetti, J. Paufique, S. Stroebele, S. Tordo, 2002, Adaptive Optical System Technologies II, SPIE **4839**, p. 1-8
8. R. Donaldson, D. Bonaccini, J. Brynnell, B. Buzzoni, L. Close, B. Delabre, C. Dupuy, J. Farinato, E. Fedrigo, N. Hubin, E. Marchetti, S. Stroebele, S. Tordo, 2000, Adaptive Optical Systems Technology, SPIE **4007**, p.82-93
9. S. Oberti, H. Bonnet, E. Fedrigo, L. Ivanescu, M. Kasper.; 2004, in "Advancements in Adaptive Optics", Vol. **5490**, p. -
10. L. Ivanescu, R. Arsenault, E. Fedrigo, M. E. Kasper, S. Oberti, J. Paufique, S. Stroebele, S. Voiron: 2004, in "Advancements in Adaptive Optics", Vol. **5490**, p. -
11. R. Arsenault, P. Kervella<sup>1</sup>, R. Donaldson, M. Kasper, E. Fedrigo, A. Wallanders, M. Schoeller, N. Housen, F. Delplancke, F. Salgado, C. Dupuy, N. Hubin, L. Ivanescu, S. Oberti, J. Paufique, S. Rossi, 2004, in "Advancements in Adaptive Optics", Vol. **5490**, p. -
12. M. Kasper, E. Fedrigo, L. Ivanescu, S. Oberti, 2004, JOSA A, vol. **21** pp. 1004-1008
13. J. Paufique, P. Biereichel, R. Donaldson, B. Delabre, E. Fedrigo, F. Franza, P. Gigan, D. Gojak, N. Hubin, M. Kasper, U. Kaeufl, J.-L. Lizon, S. Oberti, J.-F. Pirard, E. Pozna, J. Santos, S. Stroebele, 2004, in "Advancements in Adaptive Optics", Vol. **5490**, p. -